Check for updates

Received: 23 September 2021 | Revised: 20 December 2021 | Accepted: 20 December 2021

DOI: 10.1002/app.52094

ARTICLE

Applied Polymer SCIENCE WILEY

A new slit-radial die for simultaneously measuring steady state shear viscosity and first normal stress difference of viscoelastic liquids via capillary rheometry

Masood Khabazian Esfahani[1] | **Christos K. Georgantopoulos**[1] | **Ingo F. C. Naue**[1] | **Joachim Sunder**[2] | **Manfred Wilhelm**[1]

[1]Karlsruhe Institute of Technology (KIT), Institute for Chemical Technology and Polymer Chemistry (ITCP), Engesserstraße 18, Karlsruhe, Germany

[2]GÖTTFERT Werkstoff-Prüfmaschinen GmbH, Siemensstraße 2, Buchen, Germany

Correspondence
Manfred Wilhelm, Karlsruhe Institute of Technology (KIT), Institute for Chemical Technology and Polymer Chemistry (ITCP), Engesserstraße 18, 76131 Karlsruhe, Germany.
Email: manfred.wilhelm@kit.edu

Abstract

A new slit-radial die capable of simultaneously obtaining steady state shear viscosity $\eta(\dot{\gamma})$ and the average first normal stress difference coefficient $\langle\Psi_1(\dot{\gamma})\rangle$ via capillary rheometry has been developed. The steady state shear viscosity $\eta(\dot{\gamma})$ and average first normal stress difference coefficient $\langle\Psi_1(\dot{\gamma})\rangle$ are calculated in the slit part and radial part of the die, respectively. The steady state shear viscosity $\eta(\dot{\gamma})$ from the slit part of the slit-radial die is compared to shear viscosities $\eta(\dot{\gamma})$ obtained from a capillary die and also the magnitude of the complex viscosity $|\eta^*(\omega)|$ obtained from oscillatory shear experiment. The average value of first normal stress difference coefficient $\langle\Psi_1(\dot{\gamma})\rangle$ which is calculated in the radial part of the slit-radial die is compared to first normal stress difference coefficient $\Psi_1(\dot{\gamma})$ obtained from transient shear experiment in a cone-plate geometry and the molecular stress function model predictions. The effect of variation of power law fitting parameters (consistency index, k and power law index, n) on average value of the first normal stress difference coefficient $\langle\Psi_1(\dot{\gamma})\rangle$ obtained from the radial part of the slit-radial die is discussed. As this die has the shape of the city map of Karlsruhe it is named as Karlsruhe die.

KEYWORDS

extrusion, manufacturing, rheology

1 | INTRODUCTION

Under deformation, the end-to-end vector of a random coil-like polymer chain becomes oriented parallel to the flow direction. In order to reduce the stress imposed on the chains in shear flow, for example, in food or polymer melt processing, the oriented macromolecules try to return to their original random coil configuration, which in contrast to Newtonian fluids creates dissimilar diagonal stress tensor elements. To quantify this tensorial property, first and second normal stress differences are defined as $N_1 = \tau_{11}\text{-}\ \tau_{22}$ and $N_2 = \tau_{22}\text{-}\ \tau_{33}$, respectively. For viscoelastic materials the shear rate-dependent viscosity as related to shear stress τ_{12} is not enough to fully describe the fluid behavior under steady shear deformation. Hence, to fully characterize the steady shear flow,

This is an open access article under the terms of the Creative Commons Attribution-NonCommercial License, which permits use, distribution and reproduction in any medium, provided the original work is properly cited and is not used for commercial purposes.
© 2022 The Authors. *Journal of Applied Polymer Science* published by Wiley Periodicals LLC.

10974628, 2022, 18, Downloaded from https://onlinelibrary.wiley.com/doi/10.1002/app.52094 by Karlsruher Inst F. Technologie, Wiley Online Library on [20/10/2022]. See the Terms and Conditions (https://onlinelibrary.wiley.com/terms-and-conditions) on Wiley Online Library for rules of use; OA articles are governed by the applicable Creative Commons License

three material functions: (1) shear viscosity $\eta(\dot{\gamma})$, (2) first $\Psi_1(\dot{\gamma})$, and (3) second $\Psi_2(\dot{\gamma})$ normal stress difference coefficients need to be determined. These functions can be obtained from start-up shear experiment in cone-plate and plate-plate geometries. However, these experiments are limited by the instrument capability to a maximum shear rate of about 10 s^{-1} for polyethylene. At higher shear rates edge fracture pushes the material out of the plates gap. To determine material functions at higher shear rates, a partitioned cone-plate geometry was designed and described in the literature to avoid experimental imperfections of common cone-plate geometries such as wall slip, shear banding, and edge fracture to reach high steady state shear rates.[1–4]

The normal forces are responsible for die swell,[5] edge fracture,[6] and the Weissenberg or rod climbing effect.[5,7] The molecular structure of polymers also influences these properties. Die swell and melt fracture are the limiting factors in polymer production. Many industrial manufacturing processes, for example, fiber spinning, film blowing and injection molding, are limited to an upper-bound production speed due to the creation of excessive normal forces, which later lead to the extrusion flow instabilities. The effect of molecular weight, molecular weight distribution and branching on first normal stress difference of linear and branched polybutadienes was investigated by Han et al.[8] The plot of first normal stress difference against shear stress was introduced for linear and branched polybutadienes. It was found that such a plot is sensitive to molecular weight distribution and branching and does not depend on molecular weight.[8] Wood-Adams[9] investigated the effect of low levels of long chain branching in metallocene high density polyethylene on viscosity and first normal stress difference coefficient. It was concluded that the first normal stress difference coefficient was more sensitive to the presence of long chain branches than viscosity. Qualitatively, the effect of molecular structure on instabilities was studied by means of a set-up with three piezo pressure transducers (sharkskin die).[10–13] The relation between first normal stress difference N_1 and the onset of instabilities in polyethylene extrusion was also investigated.[14] The new slit-radial die has the potential to make a quantitative scale to relate the molecular structure of the polymeric liquids, for example, molecular weight, molecular weight distribution, and branching to their steady state elastic properties $(N_1(\dot{\gamma}), \Psi_1(\dot{\gamma}))$.

Different methods have so far been developed and used to measure normal stresses in polymer liquids. Baird used the pressure hole effect in a slit die to measure N_1.[15] Baird also pointed out that the effect of pressure sensor placement and its calibration after installation in the die have a profound effect on the accuracy of normal stress measurements.[15] However, Broadbent et al.[16] and Higashitani[17] put a question mark on the accuracy of calculating the derivation of the first normal stress difference from the pressure hole effect. Later, Kadar et al. used a highly sensitive piezoelectric pressure transducers to determine normal stress differences by the pressure hole effect. They showed that the first normal stress difference can be determined whereas the second normal stress difference cannot be measured within the experimental accuracy.[18] Exit pressure is also used for the determination of elastic properties of polymers melts.[19] In the exit pressure method a series of pressure transducers are installed in a die and the pressure drop is recorded along the die and is extrapolated to the die exit.[20,21] Contradictory results have been reported with respect to this method. Boger for example stated that this method is not accurate and it only gives an upper limit to parameters of the rheological material functions.[22] Tuna mentioned that extrapolating the pressure values to the die exit gave different normal force values for a linear or a quadratic fitting.[23] Tuna had to extrapolate the pressure values with a quadratic function to the die exit since the linear fit gave negative pressure values at the die exit.[23] Carreau et al.[24] claimed that due to high viscous energy dissipation or velocity rearrangement near the die exit, the exit pressures cannot be used to determine first normal stress of polymeric liquids by measuring the exit pressure effect.

Another approach to measuring normal stress differences is the application of radial flow. In this type of flow, the polymer liquid is pressurized between two circular parallel disks. By integration of the r-component of the momentum balance in cylindrical coordinate systems, Winter used the power law model to calculate the first and second normal stress difference coefficients. He assumed that the first and second normal stress difference coefficients follow a power law dependency.[25] Laurencena used the generalized Newtonian fluid equation to calculate the first normal stress difference.[26,27] Different models have been used to measure normal stresses in radial flow, for example, yield power law,[28] third order fluid,[29] Rivlin-Ericksen fluid,[30] Jeffreys[31] and Sisko's model.[32]

In the first part of our study, a new slit-radial die capable of simultaneously measuring steady state shear viscosity and average value of first normal stress difference coefficient via capillary rheometery is introduced. In the next section, the underlying theory and assumptions behind steady state viscosity and average first normal stress difference coefficient calculations are presented. The steady state viscosity $\eta(\dot{\gamma})$ from the slit part of the slit-radial die is compared to the magnitude of the complex viscosity $|\eta^*(\omega)|$ and also to the steady state shear viscosity obtained from the capillary rheometer with a capillary die with a round cross section. The average value of first normal stress difference coefficient obtained from the radial part of the slit-radial die is compared to the values obtained from transient shear experiment with a

10974628, 2022, 18, Downloaded from https://onlinelibrary.wiley.com/doi/10.1002/app.52094 by Karlsruher Inst F. Technologie, Wiley Online Library on [20/10/2022]. See the Terms and Conditions (https://onlinelibrary.wiley.com/terms-and-conditions) on Wiley Online Library for rules of use; OA articles are governed by the applicable Creative Commons License

$d = 13$ mm cone-plate geometry. Afterwards, the effect of $\pm 2\%$ variation of the power law model parameters (consistency index k and power law index n) on the average first normal stress difference coefficient values, calculated from the radial part of the slit-radial die, is presented.

2 | SLIT-RADIAL DIE DESCRIPTION

There are two types of radial flows, namely diverging and converging. In diverging type, a fluid enters at the center of two parallel disks and diverges outwards. For converging type, the fluid enters between the parallel disks at the circumference, converges inwards to the center and exits from the center. This study uses the diverging radial flow, which allows the measurement of pressures in the radial die at different distances from the center. As Figure 1 shows, the slit-radial die is composed of two halves, namely the channel and sensor halves. In the channel half the steel is machined to form the slit and radial parts of the die. For the sensor half, the surface is plain with two holes to install two gauge pressure sensors P2 and P3; P1 is the pressure sensor inside the capillary rheometer reservoir. The pressure sensors are accurately moved forward and backward by means of the supporting screws to make sure that all of them are precisely flushed on the die surface. To control the slit-radial die temperature, a K-type thermocouple connected to a PID controller is installed in the die. The heating is done by means of an electrical heating jacket around the die.

The flow in the slit and radial parts is described by Cartesian and cylindrical coordinate systems, respectively. In the slit part the flow is in the y-direction and in the radial part in the r-direction. The z axis is perpendicular to the flow direction in both the slit and radial parts (Figure 2). In Figure 2c the historic map of the city Karlsruhe is shown. Due to the resemblance of the slit radial to the city map, the slitradial die is referred to as the Karlsruhe die. In this die the polymer melt first goes through a rectangular channel before entering the radial die section. The steady state shear viscosity is calculated at the slit part by means of pressure difference between the pressure value of the pressure sensor installed in the capillary rheometer reservoir (P1) and the pressure value of the first pressure sensor installed at the entrance of the radial part (P2). The first normal stress difference is calculated at the radial part of the die by means of pressure difference between pressure sensors P2 and P3.

The pressure sensors that have been placed flashed in the slit-radial die (P2 and P3) are gauge pressure sensors.

3 | THEORETICAL BACKGROUND

3.1 | Steady state shear viscosity calculation

The steady state shear viscosity is calculated in the slit part of the die (Figure 2a). Equation (1) and Equation (2) give the apparent shear stress and apparent shear rate, respectively. The ratio of Equation (1) to Equation (2) yields the apparent steady state shear viscosity,[34] Equation (3).

$$\sigma_a = \frac{\Delta P_{slit}}{L}\frac{H}{2} \tag{1}$$

$$\dot{\gamma}_a = \frac{6Q}{H^2 W} \tag{2}$$

$$\eta_a = \frac{\sigma_a}{\dot{\gamma}_a} = \frac{\Delta P_{slit}}{L}\frac{H^3 W}{12Q} \tag{3}$$

where ΔP_{slit} is the difference in pressure at the capillary rheometer reservoir pressure sensor (P1), and at the exit of the slit part of the slit-radial die (P2), and Q is the volumetric flow rate.

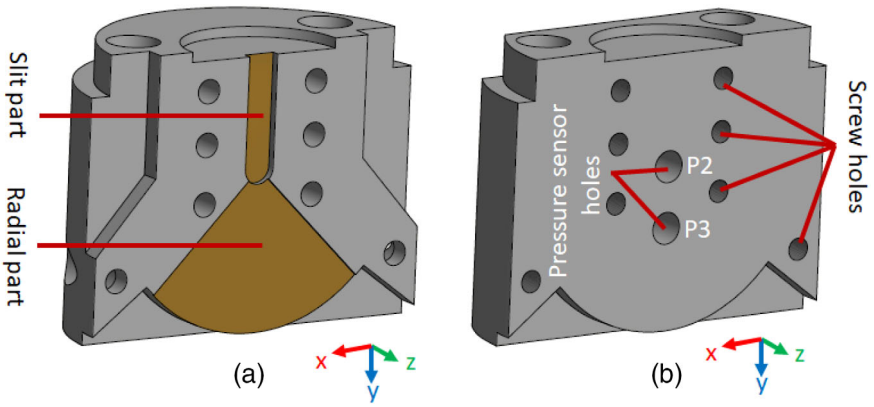

FIGURE 1 Open parts of the slit-radial die. (a) Channel half and (b) sensor half [Color figure can be viewed at wileyonlinelibrary.com]

10974628, 2022, 18, Downloaded from https://onlinelibrary.wiley.com/doi/10.1002/app.52094 by Karlsruher Inst F. Technologie, Wiley Online Library on [20/10/2022]. See the Terms and Conditions (https://onlinelibrary.wiley.com/terms-and-conditions) on Wiley Online Library for rules of use; OA articles are governed by the applicable Creative Commons License

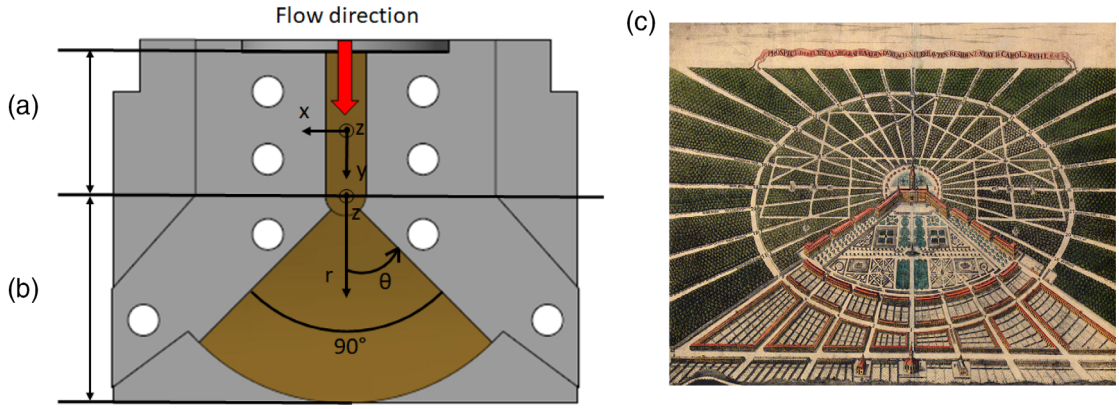

FIGURE 2 Slit-radial die. (a) Slit part (b) radial part from the view of the channel half with the cylindrical and Cartesian coordinate systems. (c) Historic map of the city Karlsruhe in 1721[33] [Color figure can be viewed at wileyonlinelibrary.com]

3.2 | Calculation of the first normal stress difference

The radial part is a quarter of a complete circle (Figure 2b).

The Cauchy momentum balance and the continuity equation in cylindrical coordinates are given by Equation (4) and Equation (5).

$$\rho\left(\frac{\partial\vec{v}}{\partial t}+\vec{v}\cdot\nabla\vec{v}\right)=-\nabla p-\nabla\cdot\underline{\underline{\tau}}+\rho\vec{g} \tag{4}$$

$$\frac{\partial\rho}{\partial t}+\frac{1}{r}\frac{\partial(\rho r v_r)}{\partial r}+\frac{\partial(\rho v_\theta)}{\partial\theta}+\frac{\partial(\rho v_z)}{\partial z}=0 \tag{5}$$

where ρ is the density, $\vec{v}$ is the velocity vector, $\underline{\underline{\tau}}$ is the stress tensor, p is pressure, $\vec{g}$ is gravitational acceleration vector and r, z, and θ are cylindrical coordinates. According to the geometry of the radial part of the slit-radial die r, z, and θ represent the flow, gradient and neutral directions, respectively. The following assumptions are applied to simplify the momentum equation:

- Steady flow, $\frac{\partial}{\partial t}(v_r,v_\theta,v_z)=0$.
- Rotational symmetry, $\frac{\partial}{\partial\theta}(v_r,v_\theta,v_z)=0$.
- Incompressible fluid, $\frac{\partial\rho}{\partial t}=0$.
- Negligible velocity in z and θ directions, $\vec{v}=(v_r,0,0)$ with $v_r=f(r,z)$.
- Creeping flow.
- No viscous heating.
- Negligible stress imposed by gravity.

Appling those assumptions, Equation (5) turns into Equation (6) for the r-component of the momentum balance Equation.

$$r-component:\ 0=-\frac{\partial p}{\partial r}-\frac{\partial\tau_{rr}}{\partial r}-\frac{\tau_{rr}-\tau_{\theta\theta}}{r}-\frac{\partial\tau_{rz}}{\partial z} \tag{6}$$

In the radial part of the slit-radial die, the first and the second normal stress differences are defined according to Equation (7) and Equation (8).

$$N_1=\tau_{rr}-\tau_{zz} \tag{7}$$

$$N_2=\tau_{zz}-\tau_{\theta\theta} \tag{8}$$

The terms $(\frac{\partial\tau_{zz}}{\partial r}-\frac{\partial\tau_{zz}}{\partial r})$ and $(\frac{\tau_{zz}}{r}-\frac{\tau_{zz}}{r})$ are added to the right hand side of Equation (6) then Equation (9) is derived.

$$0=-\frac{\partial p}{\partial r}-\frac{\partial\tau_{zz}}{\partial r}-\frac{\partial(\tau_{rr}-\tau_{zz})}{\partial r}-\frac{\tau_{zz}-\tau_{\theta\theta}}{r}-\frac{\tau_{rr}-\tau_{zz}}{r}-\frac{\partial\tau_{rz}}{\partial z} \tag{9}$$

In terms of normal stress differences, Equation (9) is rearranged to Equation (10)

$$0=\frac{\partial(p+\tau_{zz})}{\partial r}+\frac{\partial N_1}{\partial r}+\frac{N_1}{r}+\frac{N_2}{r}+\frac{\partial\tau_{rz}}{\partial z} \tag{10}$$

Relative to N1 the absolute value of second normal stress difference N_2 is assumed to be negligible. This assumption, that is, that $|N_2|<<|N_1|$, was introduced by Weissenberg for polymer solutions,[35] however, its validity is still under question. Meissner et al.[36] reported the value of $|N_2/N_1|=0.24$ for a low density polyethylene at low shear rate of $\dot{\gamma}_{app.}=0.5\,s^{-1}$ at 150°C. In his publication, Schweizer mentioned that the relative value of $|N_2/N_1|$ decreased from 0.24 at $\dot{\gamma}_{app.}=0.1\,s^{-1}$ to 0.05 at $\dot{\gamma}_{app.}=$

10974628, 2022, 18, Downloaded from https://onlinelibrary.wiley.com/doi/10.1002/app.52094 by Karlsruher Inst F. Technologie, Wiley Online Library on [20/10/2022]. See the Terms and Conditions (https://onlinelibrary.wiley.com/terms-and-conditions) on Wiley Online Library for rules of use; OA articles are governed by the applicable Creative Commons License

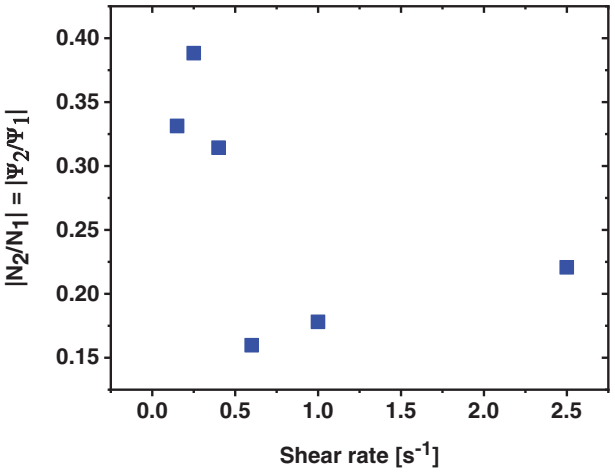

FIGURE 3 The relative absolute value of second normal stress difference over first normal stress difference of LDPE at 180°C at different shear rates [Color figure can be viewed at wileyonlinelibrary.com]

$30\,s^{-1}$ for a polystyrene at 190°C.[3] The current study assumes that $|N_2| << |N_1|$; therefore in Equation (10), $N_1/r + N_2/r$ is replaced by N_1/r. The validity of the assumption is further investigated by measuring $N_2 + N_1$ in a 13 mm plate-plate geometry. Figure 3 shows that ($|N_2/N_1|$ the absolute value of ratio of the second normal stress difference to the first normal stress difference) decreases as the shear rate increases. $|N_2/N_1|$ cannot be measured at higher shear rates since the material shear stress falls above the rheometer threshold and therefore, there is no experimental data at high shear rates for the above-mentioned ratio. It is probable that at higher shear rates ($>10\,s^{-1}$) the ratio of second normal stress difference over first normal stress difference decreases further.

The pressure sensors installed in the wall of the radial part of the slit-radial die detect the pressure value P, which is the sum of polymer melt pressure p and the normal stress τ_{zz} in z direction perpendicular to the flow direction ($P = p + \tau_{zz}$). Therefore, Equation (10) is rearranged to Equation (11).

$$\frac{\partial(rN_1)}{\partial r} = -r\frac{\partial(P)}{\partial r} - r\frac{\partial\tau_{rz}}{\partial z} \tag{11}$$

The shear stress τ_{rz} in the radial part of the die is modeled as a power law fluid according to Equation (12).

$$\tau_{rz} = k\dot{\gamma}^n = k\left(\frac{\partial v_r}{\partial z}\right)^n \tag{12}$$

where k and n are material dependent fitting parameters of the power law model. For a power law fluid in a radial die, the flow velocity v_r is expressed by Equation (13).[32]

$$v(r,z) = \frac{Q}{2\pi rh}\frac{(2n+1)}{n+1}\left[1-\left(\frac{2z}{h}\right)^{\frac{1+n}{n}}\right] \tag{13}$$

where Q is the capillary volumetric flow rate and h is the slit height in the radial part. The shear rate at the wall of the radial die is expressed by Equation (14). Because the shear rate at the wall of the radial die is radius dependent, the shear rate is replaced by an average shear rate of Equation (15) in the radial part of the slit-radial die between radius r_i to radius r_j.

$$\dot{\gamma}|_{z=\frac{h}{2}} = \frac{Q}{\pi h^2 r}\frac{(2n+1)}{n} \tag{14}$$

$$\langle\dot{\gamma}\rangle = \frac{\int_{r_i}^{r_j}\dot{\gamma}|_{z=\frac{h}{2}}dr}{r_j - r_i} = \frac{1}{r_j - r_i}\frac{Q}{\pi h^2}\frac{(2n+1)}{n}ln\left(\frac{r_j}{r_i}\right) \tag{15}$$

The last term on the right-hand side of Equation (11) is the first derivative of shear stress with respect to the z direction. In Equation (12) the shear stress is defined in terms of shear rate. Equation (16) shows the first derivative of shear stress with respect to z.

$$\frac{\partial\tau_{rz}}{\partial z} = kn\left(\frac{\partial^2 v_r}{\partial z^2}\right)\left(\frac{\partial v_r}{\partial z}\right)^{n-1} \tag{16}$$

Using Equation (13) and Equation (16), Equation (11) can be rewritten as Equation (17).

$$\frac{\partial(rN_1)}{\partial r} = -r\frac{\partial(P)}{\partial r} - 2k\frac{Q}{\pi h^3}\frac{(2n+1)}{n}\left[\frac{Q}{\pi h^2 r}\frac{2n+1}{n}\right]^{n-1} \tag{17}$$

Equation (17) is discretized over the distance between pressure sensors P2 and P3 (Equation [18]) at the wall of the radial die.

$$\frac{r_3N_1^{P3} - r_2N_1^{P2}}{r_3 - r_2} = -r_2\frac{P3 - P2}{r_3 - r_2} - 2k\frac{Q}{\pi h^3}\frac{(2n+1)}{n}\left[\frac{Q}{\pi h^2 r_2}\frac{2n+1}{n}\right]^{n-1} \tag{18}$$

where r_2 and r_3 are the discretization radii for the pressure sensors P2 and P3, respectively.

10974628, 2022, 18, Downloaded from https://onlinelibrary.wiley.com/doi/10.1002/app.52094 by Karlsruher Inst F. Technologie, Wiley Online Library on [20/10/2022]. See the Terms and Conditions (https://onlinelibrary.wiley.com/terms-and-conditions) on Wiley Online Library for rules of use; OA articles are governed by the applicable Creative Commons License

The diameter of the tip of the pressure sensors is 7.8 mm and the distance between the pressure sensors centers is 15 mm. The ratio of the distance between pressure sensors P2 and P3 to the pressure sensors tip diameter is $\frac{15}{7.8}=1.92$. Therefore, it is assumed that variation of the first normal stress difference over the distance between pressure sensors is replaced with an average value of $<N_1>$.

After simplification, Equation (18) is rewritten resulting in Equation (19).

$$\langle N_1\rangle^{P2-P3}=\left|-r_2\frac{P3-P2}{r_3-r_2}-2k\frac{Q}{\pi h^3}\frac{(2n+1)}{n}\left[\frac{Q}{\pi h^2 r_2}\frac{2n+1}{n}\right]^{n-1}\right| \tag{19}$$

For comparing and validating $<N_1>$ values obtained from the slit-radial die (Poiseuille flow) with N_1 values of transient shear experiment (Couette flow), the first normal stress difference coefficient, Ψ_1 is calculated according to Equation (20).

$$\Psi_1=\frac{N_1}{\dot{\gamma}^2} \tag{20}$$

For radial flow the average first normal stress difference coefficient, $<\Psi_1>$ is defined by Equation (21).

$$\langle\Psi_1\rangle=\frac{\langle N_1\rangle}{\langle\dot{\gamma}\rangle^2} \tag{21}$$

where $\langle\dot{\gamma}\rangle$ is the average shear rate at the wall of the radial part of the slit-radial die between pressure sensors, according to Equation (15). Therefore, Equation (22) is used to calculate the average value of the first normal stress coefficient in the radial part of the slit-radial die between the pressure sensors of P2 and P3.

$$\Psi_1{}^{P2-P3}=\frac{1}{\dot{\gamma}^2_{P2-P3}}\left|-r_2\frac{P3-P2}{r_3-r_2}-2k\frac{Q}{\pi h^3}\frac{(2n+1)}{n}\left[\frac{Q}{\pi h^2 r_2}\frac{2n+1}{n}\right]^{n-1}\right| \tag{22}$$

4 | MOLECULAR STRESS FUNCTION MODEL

The Doi-Edwards model (DE model) assumes that the polymer chain is confined in a phantom tube created by the constraints imposed by the neighboring chains. The model assumes that the chain remains in its equilibrium state during the deformation and hence the tube diameter remains constant. The DE model can therefore predict the polymer liquid behavior in shear deformation. However, in elongational flows it lacks the strain hardening behavior, which is a typical behavior of long-chain branched polymers in elongational flows.[37] Equation (23) expresses the DE model stress tensor.[38–40]

$$\sigma_{DE}(t)=\int_{-\infty}^{t}m(t-t')S^{IA}_{DE}(t,t')dt' \tag{23}$$

where $m(t–t')$ is the memory function and is defined as $m(t-t')=-\frac{dG(t-t')}{dt'}$ where $G(t)$ is the relaxation modulus, and S is the Doi-Edward orientation tensor with independent alignment assumption.

The idea of tube diameter decrease is added into the DE model in terms of molecular stress function $f(t,t')$ which is defined as the ratio of initial tube diameter a_0 to that at an arbitrary time later $a(t)$.

$$f(t,t')=\frac{a_0}{a(t)} \tag{24}$$

This way the MSF model is able to predict strain hardening behavior of long chain branched polymers in uniaxial elongational flows.[41] The stress tensor of the MSF model is expressed by Equation (25).

$$\sigma_{MSF}(t)=\int_{-\infty}^{t}m(t-t')f^2(t,t')S^{IA}_{DE}(t,t')dt' \tag{25}$$

For uniaxial elongational flow and transient shear flow, the molecular stress function f for long chain branched polymers is expressed by Equation (26) and Equation (27).

$$\frac{df^2}{dt}=\dot{\varepsilon}\frac{\beta f^2}{1+\frac{\beta-1}{f^4}}\left(S_{11}-S_{22}-\frac{f^2-1}{f^2_{max}-1}\sqrt{S_{11}+\frac{1}{2}S_{22}}\right) \tag{26}$$

$$\frac{df^2}{dt}=\dot{\varepsilon}\frac{\beta f^2}{1+\frac{\beta-1}{f^4}}\left(S_{12}-\frac{f^2-1}{2\left(f^2_{max}-1\right)}\sqrt{S_{11}+\frac{1}{2}S_{22}}-\frac{a_2(f^2-1)}{2}\sqrt{|S_{11}-S_{22}|}\right) \tag{27}$$

where $f(t)$ is the molecular stress function. The Currie approximation[42] is used to calculate the orientation tensor S elements. The MSF model has three fitting parameters, namely β, f_{max} and a_2. In Equation (26), β represents the ratio of total number of segments in a molecule to the number of segments in the polymer backbone of a branched topology. The parameter β governs the slope of

10974628, 2022, 18, Downloaded from https://onlinelibrary.wiley.com/doi/10.1002/app.52094 by Karlsruher Inst F. Technologie, Wiley Online Library on [20/10/2022]. See the Terms and Conditions (https://onlinelibrary.wiley.com/terms-and-conditions) on Wiley Online Library for rules of use; OA articles are governed by the applicable Creative Commons License

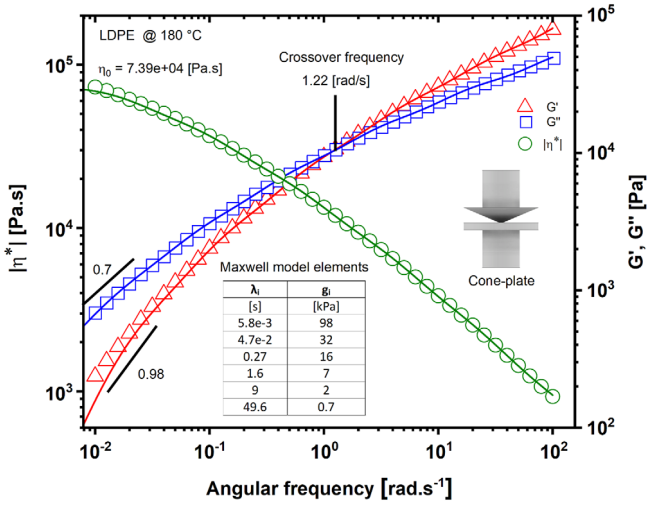

FIGURE 4 Storage, loss moduli, and magnitude of complex viscosity of LDPE fitted with a 6-element Maxwell model at 180°C [Color figure can be viewed at wileyonlinelibrary.com]

strain hardening and f_{max} determines the steady state viscosity in uniaxial elongational flow.[43,44] In transient shear experiment, a_2 is a fitting parameter. In order to calculate the MSF model prediction in uniaxial elongational flow, the relaxation modulus $G(t)$ is calculated by fitting the Maxwell model on oscillatory shear data. The Maxwell model elements are reported in Figure 4.

5 | MATERIAL AND EXPERIMENTS

In this part the rheological properties of a low density polyethylene (LDPE) were determined as a proof of concept of the new slit-radial die. The LDPE molecular properties are listed in Table 1. The experimental procedure for the full rheological characterization of this specific LDPE is elaborated via oscillatory and elongational experiments.

Frequency sweep experiment was performed with an ARES G2 rheometer with 13 mm plate-plate geometry with 1 mm gap at 180°C in the angular frequency window of $\omega = 0.01$ to $\omega = 100$ rad.s^{-1}. The relaxation moduli were then fitted with a 6-element Maxwell model.

Start-up shear experiments were performed with an ARES G2 rheometer with 13 mm common cone-plate geometry (cone angle $\alpha = 0.1$ rad) at 180°C. The samples were cut out of a 1 mm thick sheet which had already been pressed at 10 bar at 180°C for 10 min and cooled down under the same pressure to room temperature.

Start-up elongational tests are done by an extensional viscosity fixture (EVF) in an ARES G2 rheometer at 180°C. The sample, in the form of granules, was pressed at 10 bar at 180°C for 10 min and cooled down under the same pressure to room temperature. The samples were cut out in a rectangular sheet with 1 mm thickness, 15 mm length, and 10 mm height.

Capillary rheological experiments were carried out using at Goettfert Rheograph (RG) 50 kN capillary rheometer. The sample was loaded in the capillary rheometer reservoir (30 mm reservoir diameter) and heldfor 15 min at 180°C to ensure thermal equilibrium was reached. Three capillary (round cross-section area) dies with diameter of $D = 2$ mm and length of $L = 10$, 20 and 30 mm were used. The Bagley and Rabinowitsch-Weissenberg corrections were applied to the pressure data obtained by the three capillary dies. This report presents the corrected experimental data obtained by the capillary die with $D = 2$ mm and $L = 30$ mm.

6 | RESULTS AND DISCUSSION

In this section the experimental results of the investigated LDPE are presented. The molecular stress function (MSF) was used to fit transient extensional viscosity and transient shear viscosity and predict transient first normal stress difference.

The $<\Psi_1>$ obtained from the slit-radial die are compared to the steady state values obtained from transient shear experiment and the MSF model predictions.

Figure 4 shows the frequency sweep test of LDPE between $\omega = 0.01$ (rad.s^{-1}) and $\omega = 100$ (rad.s^{-1}) at 180°C. In this frequency window, at this temperature, the material did not reach the terminal zone. The relaxation moduli of the investigated LDPE were fitted with a 6-element Maxwell model (Figure 4). The relaxation spectrum is later utilized with the MSF model.

Figure 5a depicts the transient extensional viscosity from $\dot{\varepsilon} = 0.1$ to $\dot{\varepsilon} = 2.5\,s^{-1}$. It is observed that the LDPE transient extensional viscosities present a strain hardening factor (SHF), which is the ratio of the maximum elongational viscosity to the linear viscoelastic viscosity at the same time, of about SHF = 9. The data are fitted by the MSF model, Equation (25), the fitting parameters are $\beta = 2.5$ and $f_{max} = 7$. The MSF model prediction for elongational viscosities displayed agreement with experimental data. Figure 5b shows transient shear viscosity of the LDPE between shear rates of $\dot{\gamma} = 0.1$ and $\dot{\gamma} = 2.5\,s^{-1}$. The MSF model is fitted to transient shear viscosity with fitting parameters of $\beta = 2.5$, $f_{max} = 7$ (taken from uniaxial elongational tests), and $a_2 = 0.1$. In transient shear, the MSF model well predicts the stress overshoot. For steady state viscosity, the MSF model at shear rates 2.5 and 1 s^{-1} over predicts the steady state viscosity which is due to the material getting out of the cone-plate

10974628, 2022, 18, Downloaded from https://onlinelibrary.wiley.com/doi/10.1002/app.52094 by Karlsruher Inst F. Technologie, Wiley Online Library on [20/10/2022]. See the Terms and Conditions (https://onlinelibrary.wiley.com/terms-and-conditions) on Wiley Online Library for rules of use; OA articles are governed by the applicable Creative Commons License

TABLE 1 Molecular characterization of LDPE

Material	M_n (kg/mol)	M_w (kg/mol)	PDI	η_0 at 180°C (pa.s)	ρ at 25°C (g/cm^3)	MFR ASTM D1238 (190°C/2.16 kg) [g/10 min]
LDPE	24.2	330.2	13.6	73,900	0.92	0.33

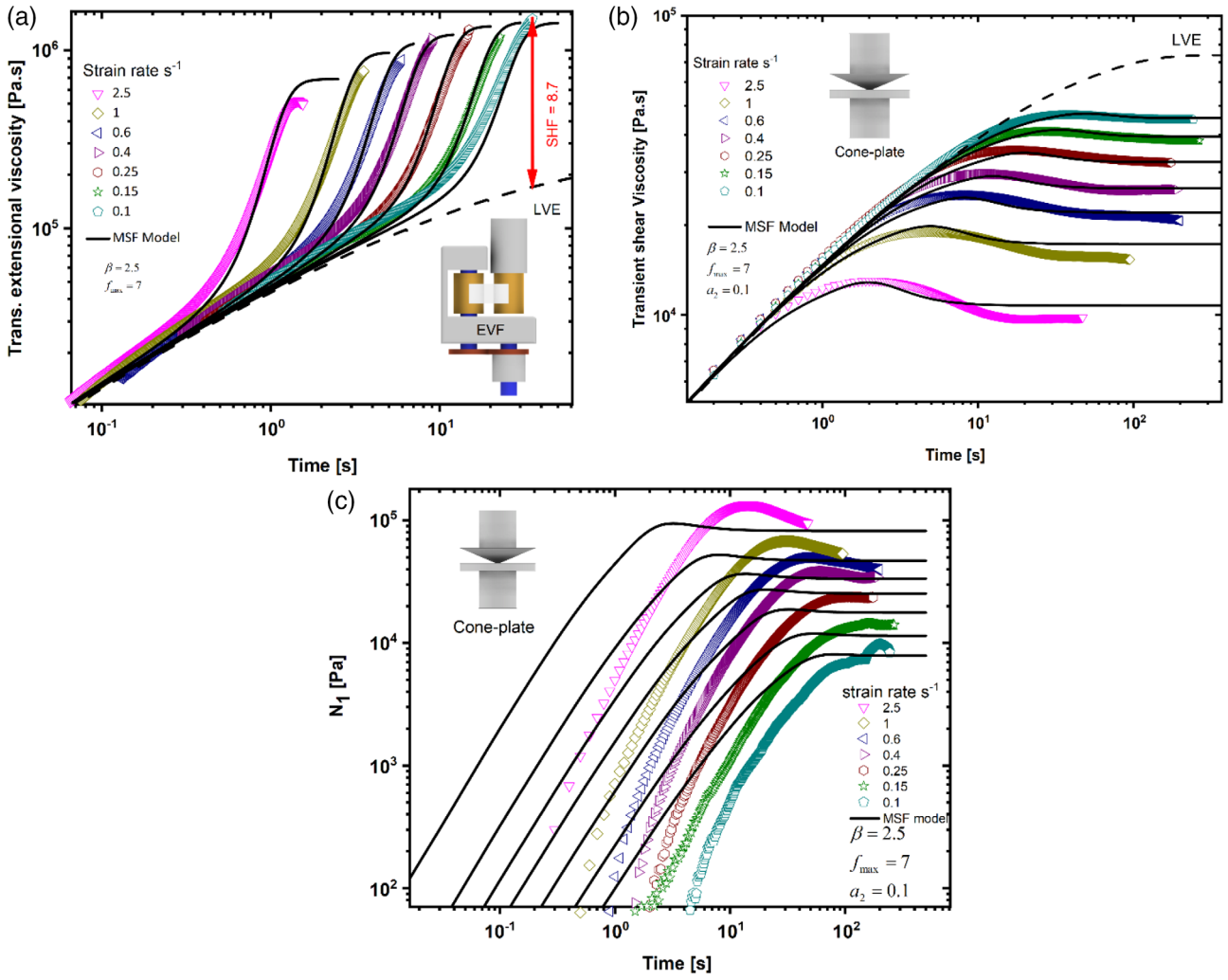

FIGURE 5 (a) Transient extensional viscosity obtained by EVF fixture in ARES G2 rheometer (b) transient shear viscosity and (c) transient first normal stress difference as they are determined via 13 mm cone-plate geometry of the investigated LDPE at different strain rates at 180°C. The connected lines are the MSF model fittings and predictions [Color figure can be viewed at wileyonlinelibrary.com]

gap. The prediction of the MSF model at shear rates below 1 s^{-1} falls on the experimental data. In Figure 5c transient first normal stress difference is depicted for shear rates between $\dot{\gamma} = 0.1$ to $\dot{\gamma} = 2.5\,s^{-1}$, the steady state value of N_1 is obtained from the plateau region. For shear rates $\dot{\gamma} = 2.5$ and $\dot{\gamma} = 1\,s^{-1}$ the edge fracture occurred before reaching the steady state. Hence, as an approximation, the final value of N_1 vs time is taken as the steady state value. The MSF model predictions with the fitting parameters of $\beta = 2.5$, $f_{max} = 7$, and $a_2 = 0.1$ are also presented. The MSF model predictions for steady state first normal stress difference gives the displayed agreement to the experimental results. The MSF model prediction in transient region have a time lag with experimental data. Time lag is defined as the time difference in which the stress overshoot happens for the experimental data and for the MSF model prediction. This happens at all the strain rates. The time lag is reported for extended interchain pressure model[45] which is a modification to the MSF model.[2]

The values of shear stress, viscosity, first normal stress difference and first normal stress difference

10974628, 2022, 18, Downloaded from https://onlinelibrary.wiley.com/doi/10.1002/app.52094 by Karlsruher Inst F. Technologie, Wiley Online Library on [20/10/2022]. See the Terms and Conditions (https://onlinelibrary.wiley.com/terms-and-conditions) on Wiley Online Library for rules of use; OA articles are governed by the applicable Creative Commons License

coefficient obtained by transient shear experiment are depicted in Figure 6. For the LDPE in transient shear experiment, for shear rates above $\dot{\gamma} = 2.5\,s^{-1}$ the measured torque becomes greater than the upper threshold of the rheometer torque limit (0.2 N.m) and therefore measuring shear stress at higher shear rates than $\dot{\gamma} = 2.5\,s^{-1}$ is not possible for 13 mm common cone-plate geometry. For shear rates lower than $\dot{\gamma} = 0.1\,s^{-1}$ the material normal force falls below the sensitivity of the rheometer normal force transducer which consequently leads to data fluctuations for Ψ_1. To overcome the shortcomings of transient shear experiment at shear rates above $\dot{\gamma} = 2.5\,s^{-1}$, this study introduces a new slit-radial die which is able to measure the average value of Ψ_1 at higher average shear rates in its radial part (Figure 1).

Table 2 reports the steady state pressure values of the capillary rheometer pressure sensor P1 and slit-radial die pressure sensors P2 and P3 at different volumetric flow rates.

The apparent shear rate of the slit part of the slit-radial die is given by Equation (2). The steady state viscosity in the slit part of the slit-radial die is calculated according to Equation (3).

In Figure 7, the magnitude of complex and steady state viscosity of LDPE obtained from three different methods are compared: oscillatory shear, capillary rheometry (capillary die, $D = 2$ mm, $L = 30$ mm), and slit-radial die. To check the data reproducibility, the experiment was repeated 3 times.

Figure 8 shows the relation between first normal stress difference coefficient Ψ_1 and shear rate obtained from

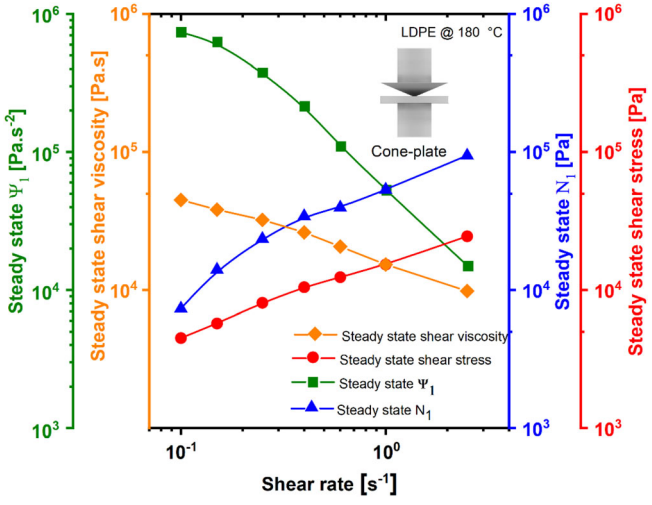

FIGURE 6 Relation between steady state Ψ_1, steady state shear viscosity, steady state N_1, steady state shear stress as a function of shear rate for a specific LDPE at shear rates between 0.1 to 2.5 s^{-1} obtained by 13 mm cone-plate geometry in ARES G2 rheometer at 180°C [Color figure can be viewed at wileyonlinelibrary.com]

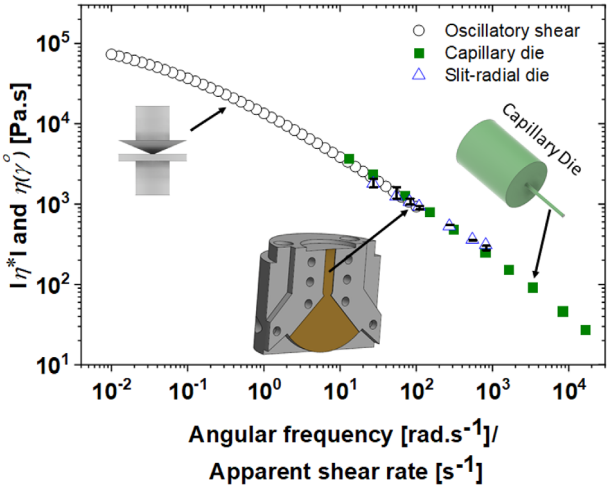

FIGURE 7 Magnitude of complex viscosity and steady state shear viscosity versus angular frequency/apparent shear rate of the LDPE at 180°C. (The black circles are taken from oscillatory shear experiments, the green squares are data from capillary rheometer with a round die, the blue triangles are steady state viscosity from the slit part of the slit-radial die) [Color figure can be viewed at wileyonlinelibrary.com]

TABLE 2 Pressure values at each pressure sensor as a function of volumetric flow rate and shear viscosity calculated from the slit part of the slit-radial die

Q (mm^3/s)	P1 (bar)	P2 (bar)	P3 (bar)	Apparent shear rate of the slit part of the die (s^{-1})	Viscosity calculated from the slit part (Pa.s)
35.3	85.6	54.8	26.0	27.17	1805
70.6	118.5	75.8	35.7	54.35	1249
105.9	147.7	93.0	43.8	81.52	1068
141.3	171.1	107.2	50.6	108.7	935.4
353.2	257	166	79.6	271.7	533.2
706.5	349	225	111	543.4	363.3
1059	424.5	267	137.6	815.2	310.4

10974628, 2022, 18, Downloaded from https://onlinelibrary.wiley.com/doi/10.1002/app.52094 by Karlsruher Inst F. Technologie, Wiley Online Library on [20/10/2022]. See the Terms and Conditions (https://onlinelibrary.wiley.com/terms-and-conditions) on Wiley Online Library for rules of use; OA articles are governed by the applicable Creative Commons License

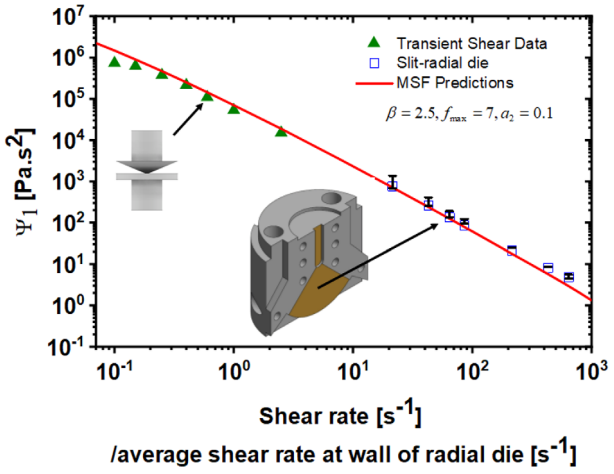

FIGURE 8 $<\Psi_1>$ versus shear rate/average shear rate at the wall of the radial part of the slit-radial die of LDPE at 180°C. (The green triangles are transient shear data at steady state taken from transient shear experiment with 13 mm diameter cone-plate geometry. The blue squares are calculated $<\Psi_1>$ from the radial part of the slit-radial die. The red line is the MSF model predictions. The presented set up extends the cone-plate measurements by about 2.5 decades [Color figure can be viewed at wileyonlinelibrary.com]

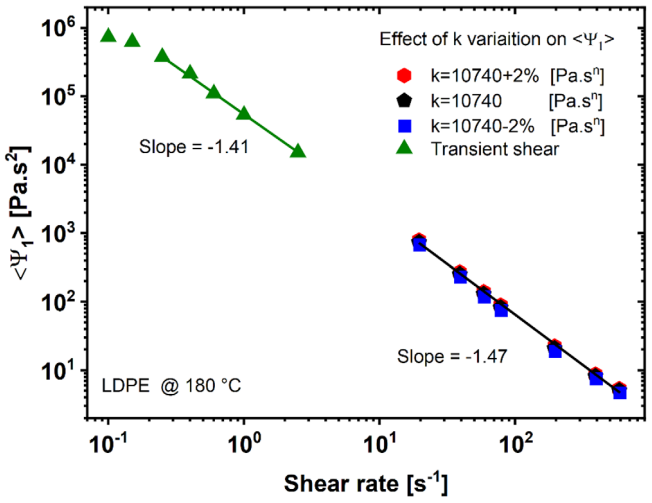

FIGURE 9 Effect of 2% variation of power-law model parameter k on $<\Psi_1>$ [Color figure can be viewed at wileyonlinelibrary.com]

transient shear experiment at steady state (green squares) and calculated average first normal stress difference coefficient $<\Psi_1>$ versus average shear rate at the wall of the radial part of the slit-radial die. To check the data reproducibility, the experiment was repeated three time. The $<\Psi_1>$ at the wall of the radial part of the slit-radial die was obtained as a result of discretization of Equation (17) over the pressure sensors P2 and P3, Equation (22).

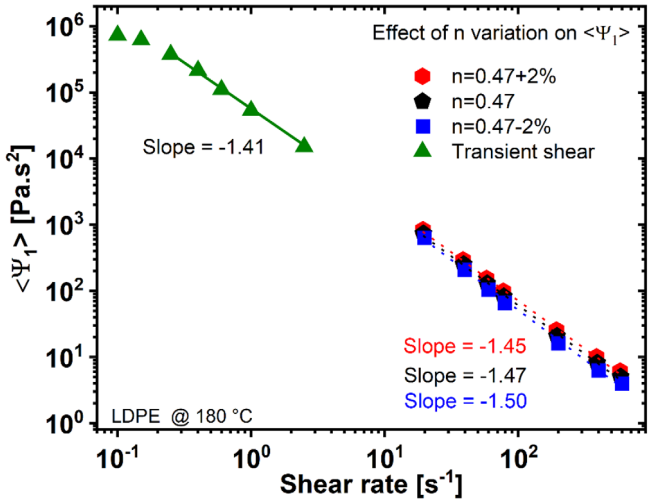

FIGURE 10 Effect of 2% variation in the power-law model parameter n on $<\Psi_1>$ [Color figure can be viewed at wileyonlinelibrary.com]

7 | EFFECT OF VARIATION OF THE POWER LAW PARAMETERS ON THE AVERAGE Ψ_1

As indicated by Equation(12) and Equation (19), the power law model parameters strongly affect the average value of the first normal stress difference coefficient $<\Psi_1>$ calculated in the radial part of the die. The effect of the power law parameters on $<\Psi_1>$ taken from radial part of the slit-radial die is illustrated in Figure 9 for $k \pm 2\%$ and in Figure 10 for $n \pm 2\%$. The power law parameters are calculated by fitting the power law model $(\eta(\dot{\gamma}) = k\dot{\gamma}^{n-1})$ on steady state viscosity versus shear rate data taken from the slit part of the slit-radial die ($n = 0.47$ and $k = 10{,}740$). *Figure 9* indicates that variation in k does not change the slope of $\log(<\Psi_1>)$ vs $\log(<\dot{\gamma}>)$.

Figure 10 depicts the effect of $\pm$ 2% variation of the power law parameter, n on the average value of Ψ_1. The results show that the change in n value by 2% changes the slope of the curve by 3.5%. The results for the investigated LDPE show that 2% variation in n constant leads to about 7% variation in average value of Ψ_1 in the investigated average shear rate interval.

8 | CONCLUSIONS

According to the new experimental slit-radial die adaptable to capillary rheometer, experimental protocols on a LDPE sample and the modeling of the flow, the following points can be drawn:

10974628, 2022, 18, Downloaded from https://onlinelibrary.wiley.com/doi/10.1002/app.52094 by Karlsruher Inst F. Technologie, Wiley Online Library on [20/10/2022]. See the Terms and Conditions (https://onlinelibrary.wiley.com/terms-and-conditions) on Wiley Online Library for rules of use; OA articles are governed by the applicable Creative Commons License

- The new slit-radial die for the capillary rheometer is capable of simultaneously measuring the steady state shear viscosity $\eta(\dot{\gamma})$ and the average value of first normal stress difference N_1 in a very simple way.
- For the studied LDPE, the average values of the first normal stress difference coefficient obtained from the slit-radial die at high shear rates follows the trend of the first normal stress difference coefficient (monotonically decreasing with increasing shear rate) obtained from transient shear experiment at low shear rates.
- The average values of the first normal stress difference coefficient obtained from the slit-radial die at high shear rates matches the MSF model prediction for the investigated LDPE.
- The effect of power law parameters (consistency index k and power law index n) by $\pm$ 2% variation on the $<\Psi_1>$ as a function of average shear rate shows that the change in k values only vertically shifts the $<\Psi_1>$ as a function of average shear rate, however, n values variation, changes the slope of the average values of Ψ_1 versus average shear rate. For this reason, the fitting of a power law model to the viscosity data obtained by the slit-radial to obtain the proper k and n values has crucial importance for the calculation of the $<\Psi_1>$. The results for the investigated LDPE show that 2% variation in n constant leads to about 7% variation in average value of Ψ_1 in the investigated average shear rate interval.

ACKNOWLEDGMENTS

Dr. Masood K. Esfahani acknowledge, Zentrales Innovationsprogramm Mittelstand (ZIM) for funding ZF4016104SY8 project. Christos K. Georgantopoulos acknowledge Pirelli Tyres S. p. A. for financial support and Dr. Andrea Causa for fruitful discussions. Dow chemicals is acknowledged for the donation of the LDPE sample. The authors thank Dr. Michael Pollard for proofreading the manuscript. The authors would like to thank GÖTTFERT Werkstoff-Prüfmaschinen GmbH for this collaboration. Open Access funding enabled and organized by Projekt DEAL.

DATA AVAILABILITY STATEMENT

No. Research data are not shared.

ORCID

Masood Khabazian Esfahani https://orcid.org/0000-0003-0947-4010

REFERENCES

[1] S. Costanzo, G. Ianniruberto, G. Marrucci, D. Vlassopoulos, *Rheol. Acta* **2018**, *363*, 57.
[2] E. Narimissa, T. Schweizer, M. H. Wagner, *Rheol. Acta* **2020**, *487*, 59.
[3] T. Schweizer, *Rheol. Acta* **2002**, *337*, 41.
[4] R. H. Ewoldt, M. T. Johnston, L. M. Caretta, in *Complex Fluids in Biological Systems: Experiment, Theory, and Computation* (Ed: S. E. Spagnolie), Springer, **2015**.
[5] R. I. Tanner, *J. Polym. Sci. Part A-2: Polym. Phys.* **1970**, *8*, 2067.
[6] S. Skorski, P. D. Olmsted, *J. Rheol.* **2011**, *1219*, 55.
[7] M. Yamamoto, *J. Phys. Soc. Jpn.* **1958**, *1200*, 13.
[8] C. D. Han, M. S. Jhon, *J. Appl. Polym. Sci.* **1986**, *3809*, 32.
[9] P. M. Wood-Adams, *J. Rheol.* **2001**, *203*, 45.
[10] H. Palza, I. F. C. Naue, M. Wilhelm, *Macromol. Rapid Commun.* **2009**, *1799*, 30.
[11] I. F. C. Naue, R. Kádár, M. Wilhelm, *Macromol. Mater. Eng.* **2015**, *1141*, 300.
[12] C. K. Georgantopoulos, M. K. Esfahani, C. Botha, I. F. C. Naue, N. Dingenouts, A. Causa, R. Kádár, M. Wilhelm, *Macromol. Mater. Eng.* **2021**, *2000801*, 306.
[13] C. K. Georgantopoulos, M. K. Esfahani, C. Botha, M. A. Pollard, I. F. C. Naue, A. Causa, R. Kádár, M. Wilhelm, *Phys. Fluids* **2021**, *093108*, 33.
[14] H. Palza, I. F. C. Naue, S. Filipe, A. Becker, J. Sunder, A. Göttfert, M. Wilhelm, *Kautsch. Gummi Kunstst.* **2010**, *456*, 10.
[15] D. G. Baird, *J. Non-Newtonian Fluid Mech.* **2008**, *13*, 148.
[16] J. M. Broadbent, A. Kaye, A. S. Lodge, D. G. Vale, *Nature* **1968**, *55*, 217.
[17] K. Higashitani, W. G. Pritchard, *Trans. Soc. Rheol.* **1972**, *687*, 16.
[18] R. Kádár, I. F. C. Naue, M. Wilhelm, *Polymer* **2016**, *193*, 104.
[19] N. Y. Tuna, B. A. Finlayson, *J. Rheol.* **1984**, *79*, 28.
[20] C. D. Han, M. Charles, W. Philippoff, *Trans. Soc. Rheol.* **1970**, *393*, 14.
[21] D. Tang, F. H. Marchesini, L. Cardon, D. R. D'hooge, *J. Rheol.* **2020**, *64*, 739.
[22] D. V. Boger, M. M. Denn, *J. Non-Newtonian Fluid Mech.* **1980**, *163*, 6.
[23] N. Y. Tuna, B. A. Finlayson, *J. Rheol.* **1988**, *285*, 32.
[24] P. J. Carreau, L. Choplin, J.-R. Clermont, *Polym. Eng. Sci.* **1985**, *669*, 25.
[25] H. H. Winter, *Polym. Eng. Sci.* **1975**, *460*, 15.
[26] B. R. Laurencena, M. C. Williams, *Trans. Soc. Rheol.* **1974**, *331*, 18.
[27] M. C. H. Lee, M. C. Williams, *J. Non-Newtonian Fluid Mech.* **1976**, *343*, 1.
[28] R. Majidi, S. Z. Miska, R. Ahmed, M. Yu, L. G. Thompson, *J. Pet. Sci. Eng.* **2010**, *334*, 70.
[29] R. B. Bird, *Appl. Sci. Res.* **1977**.
[30] W. H. Schwarz, C. Bruce, *Chem. Eng. Sci.* **1969**, *399*, 24.
[31] M. C. H. Lee, M. C. Williams, *J. Non-Newtonian Fluid Mech.* **1976**, *323*, 1.
[32] T. Y. Na, A. G. Hansen, *Int. J. Non-Linear Mech.* **1967**, *261*, 2.
[33] Information on the city of Karlsruhe, Karlsruhe Institute of Technology (KIT), xafs16.ine.kit.edu/85.php.
[34] G. Schramm, *A practical approach to rheology and rheometry*, Haake, **1994**.
[35] Weissenberg, K. *International Congress on Rheology*, **1948**.
[36] J. Meissner, R. W. Garbella, J. Hostettler, *J. Rheol.* **1989**, *843*, 33.
[37] M. Doi, S. Edwards, *Theory of polymer dynamics*, Oxford University Press, **1986**.
[38] M. Doi, S. F. Edwards, *J. Chem. Soc., Faraday Trans. 2* **1978**, *1789*, 74.

10974628, 2022, 18, Downloaded from https://onlinelibrary.wiley.com/doi/10.1002/app.52094 by Karlsruher Inst F. Technologie, Wiley Online Library on [20/10/2022]. See the Terms and Conditions (https://onlinelibrary.wiley.com/terms-and-conditions) on Wiley Online Library for rules of use; OA articles are governed by the applicable Creative Commons License

[39] M. Doi, S. F. Edwards, *J. Chem. Soc., Faraday Trans. 2* **1978**, *1802*, 74.
[40] M. Doi, S. F. Edwards, *J. Chem. Soc., Faraday Trans. 2* **1978**, *1818*, 74.
[41] M. H. Wagner, H. Bastian, P. Hachmann, J. Meissner, S. Kurzbeck, H. Münstedt, F. Langouche, *Rheol. Acta* **2000**, *97*, 39.
[42] P. K. Currie, *J. Non-Newtonian Fluid Mech.* **1982**, *53*, 11.
[43] M. H. Wagner, M. Yamaguchi, M. Takahashi, *J. Rheol.* **2003**, *779*, 47.
[44] V. Rolón-Garrido, M. Wagner, *Rheol. Acta* **2007**, *583*, 46.
[45] M. H. Wagner, *J. Non-Newtonian Fluid Mech.* **2015**, *121*, 222.

How to cite this article: M. Khabazian Esfahani, C. K. Georgantopoulos, I. F. C. Naue, J. Sunder, M. Wilhelm, *J. Appl. Polym. Sci.* **2022**, *139*(18), e52094. https://doi.org/10.1002/app.52094

10974628, 2022, 18, Downloaded from https://onlinelibrary.wiley.com/doi/10.1002/app.52094 by Karlsruher Inst F. Technologie, Wiley Online Library on [20/10/2022]. See the Terms and Conditions (https://onlinelibrary.wiley.com/terms-and-conditions) on Wiley Online Library for rules of use; OA articles are governed by the applicable Creative Commons License